17th World Conference on Earthquake Engineering, 17WCEE
Sendai, Japan - September 13th to 18th 2020

NUMERICAL MODELLING OF THE FRICTION PENDULUM SYSTEM INCORPORATING STATIC FRICTION AT BREAKAWAY

V. Quaglini[(1)], E. Gandelli[(2)], M. Penati[(3)], E. Miglio[(4)], P. Dubini[(5)]

[(1)] *Associate Professor, Politecnico di Milano, Department of Architecture, Built Environment and Construction Engineering, virginio.quaglini@polimi.it*
[(2)] *Research Fellow, Politecnico di Milano, Department of Architecture, Built Environment and Construction Engineering, emanuele.gandelli@polimi.it*
[(3)] *Research Fellow, Politecnico di Milano, Department of Mathematics "F. Brioschi", mattia.penati@polimi.it*
[(4)] *Associate Professor, Politecnico di Milano, Department of Mathematics "F. Brioschi", edie.miglio@polimi.it*
[(5)] *Research Fellow, Politecnico di Milano, Department of Architecture, Built Environment and Construction Engineering, paolo.dubini@polimi.it*

Abstract

The increasing use of sliding bearings with curved surfaces, like the Friction Pendulum System® (FPS), to implement the base isolation design in constructions, benefits from the improvement of numerical models able to capture their experimental behavior and enhance the predictive capability of nonlinear response history analyses. An effective implementation of the static, or breakaway, friction of sliding bearings in object-oriented software for structural analysis has not yet been achieved, and the use of dynamic friction only is a common practice in design. The formulation proposed in this study aims at filling the gap, by incorporating in an established numerical framework the change in the coefficient of friction occurring at the transition from the sticking, or pre-sliding phase to the dynamic sliding motion.

First, a mathematical formulation is developed in order to address the variability of the coefficient of friction based on experimental data that can be retrieved from laboratory tests on FPS bearings. The proposed "BVNC" formulation accounts for variation in the coefficient of friction with the instantaneous change of axial load and velocity, and with the amount of energy dissipated during cyclic motion; eventually, it incorporates as a new feature the static friction developed at the breakaway and at any temporary sticking between the sliding surfaces when velocity is null.

The novel formulation is hence coded in the object-oriented finite element software OpenSees by modifying the standard "SingleFPSimple3d" element which reproduces the behavior of the FPS comprising one concave sliding surface and a spherical articulation. The hysteretic force – displacement characteristics of the FPS in the horizontal direction is mathematically modelled using the theory of plasticity, and two distinct yield thresholds with a trigger condition are introduced to account for either static or dynamic friction. Other features of the model are the variation of dynamic friction with axial load and velocity, and its degradation during cyclic motion.

The primary assumptions in the development of the friction model and the verification of the new FPS element are validated in a code-to-code comparison with the standard OpenSees element. A case study relevant to a base-isolated reinforced concrete frame demonstrates the improved prediction capability of the new element over its standard counterpart, such as estimating a +40% increase in superstructure drift and column shear force and a +58% increase in isolators displacement during high intensity, Basic Design earthquakes, and up to a +130% increase in internal forces and deformations of the structure under Serviceability Design earthquakes as a consequence of not-engagement of the FPS during small-to-medium magnitude events.

Keywords: Friction Pendulum System, static coefficient of friction, OpenSees, time history analyses, friction model

1. Introduction

The Friction Pendulum System®, or FPS® [1-3], is one of the most popular isolation hardware worldwide owing to its inherent simplicity; indeed, it provides the four main functions required to the isolation system, i.e. load-bearing capability, lateral flexibility, energy dissipation and re-centering, in a single, compact design. In its basic configuration the FPS consists of a concave sliding plate and an articulated slider. The slider surface facing the concave plate is lined with a low-friction material, thus creating a sliding interface which accommodates the horizontal displacement of the superstructure (Fig. 1). Though improved versions with multiple sliding surfaces have been recently proposed [4-5], their mechanical behavior follows the same fundamental principles. Number of sliding interfaces, coefficient of friction and radius of curvature determine the isolator's performance: the concave surface provides a restoring force that is proportional to the horizontal displacement, and the friction force developed during the accommodated sliding motion provides energy dissipation that reduces the force and the displacement demand, but increases the amount of residual displacement.

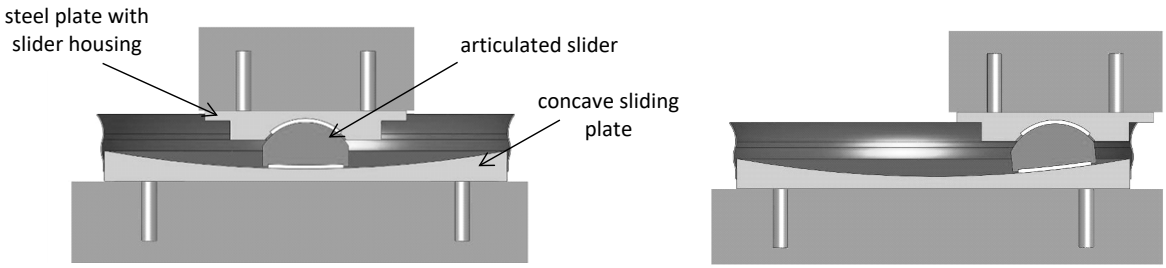

Fig. 1 – Operation of the FPS: (a) undeformed configuration; (b) deformed configuration; from [6]

Thermoplastic materials like e.g., PTFE [7], Ultra High Molecular Weight (UHMWPE) [8], and Polyamide (PA) [9] have been used as lining materials for the slider. Their coefficient of friction is affected from a number of factors, including the pressure and the velocity of sliding, the temperature, the roughness of the mating surface, and the wear and contamination of the sliding surfaces [10-15]. The typical variation of the coefficient of friction with velocity and pressure is illustrated in Fig. 2.

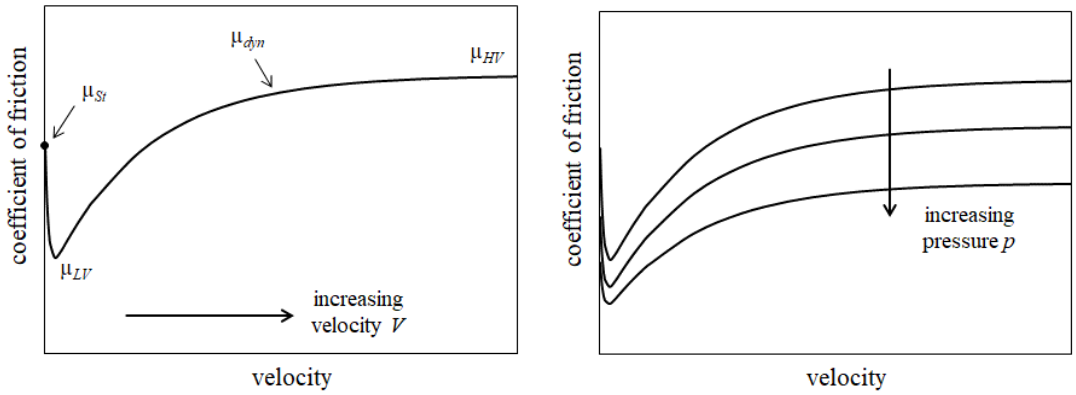

Fig. 2 – Variation of coefficient of friction of thermoplastic materials with velocity and pressure; from [6]

Here μ_{st} is the static, or pre-sliding, coefficient of friction, and μ_{dyn} is the dynamic coefficient of friction observed during sliding; μ_{dyn} in turn changes with velocity, varying from a minimum value μ_{LV} at very low velocity to a maximum value μ_{HV} at high speeds. Static friction affects the sliding interface during

© The 17th World Conference on Earthquake Engineering

dwelling, and at any temporary sticking. The static coefficient of friction during dwelling is denoted as the breakaway coefficient μ_B. As sliding starts, the frictional resistance has a steep decrease, and μ_B has been reported to be 1.5 to 4.5 times larger than μ_{LV} [9, 14, 16]. The dynamic friction also tends to decrease during sustained motion, owing to the heating of the sliding surface provided from energy dissipation [17-19], which induces the melting of a thin layer of the thermoplastic liner material that behaves a solid lubricant. The variation of the dynamic coefficient of friction with velocity and pressure has been coded in software programs for structural analysis such as SAP2000 [20], OpenSees [21] and 3D-BASIS-ME [22]. On the contrary, though some models additionally incorporating the effect of heating have been proposed [19, 23], they are not popular among researchers and practitioners. Eventually, a general model suitable for numerical analyses accounting for the static friction at breakaway is still missing [24].

A novel friction model that incorporates the effects of normal load, velocity and heating, and includes the static coefficient of friction at breakaway as a new feature is presented in this paper. This formulation is incorporated in a FPS element coded in the object-oriented finite element Open Sees software. A case study enlightens the advantages of the new element and the expected enhancement in the prediction capability of an ensuing response history analysis.

2. Numerical formulation

2.1 Physical model

The *SingleFPSimple3d* element coded in the finite element software OpenSees [25] describes the behavior of the FPS with a concave sliding surface and an articulated slider shown in Fig. 1. The element has two nodes and twelve degrees of freedom. The first node (*i*-Node) is placed at the center of the concave surface and the second node (*j*-Node) at the center of the spherical housing of the slider. The degrees of freedom in the global and the local coordinate systems are shown in Fig. 3(a): the isolator can displace in six directions, namely, translate in the vertical and in two horizontal directions, twist about the vertical axis, and rotate about two horizontal axes. The slider is rigid in the vertical direction, but its vertical rigid-body motion accompanies the displacement in the horizontal direction.

The response of the FPS can be more effectively represented in the basic coordinate system defined in Fig. 3(b). Here, the *x*-axis links the centers of curvature of the lower and upper concave surfaces (*Ci*- and *Cj*-points, respectively), and the *y*- and *z*-axes follow the right-hand rule. In such representation, the bearing has six degrees of freedom that correspond to the relative displacements and rotations between the auxiliary *Ci*- and *Cj*-Nodes, and the force – deformation behavior is formulated by assuming that the auxiliary nodes are linked by six springs that represent the mechanical behavior in the basic directions of the element: Axial, Shear 1, Shear 2, Torsion, Rotation1, and Rotation2. Indeed, in such basic representation the general expression of the element stiffness matrix is [26]:

$$[K_b]=\begin{bmatrix} Axial & 0 & 0 & 0 & 0 & 0 \\ 0 & Shear1 & Shear21 & 0 & 0 & 0 \\ 0 & Shear12 & Shear2 & 0 & 0 & 0 \\ 0 & 0 & 0 & Torsion & 0 & 0 \\ 0 & 0 & 0 & 0 & Rotation1 & 0 \\ 0 & 0 & 0 & 0 & 0 & Rotation2 \end{bmatrix} \quad (1)$$

The *SingleFPSimple3d* element has coupled friction properties with post-yield stiffening owing to the concave surface for the shear deformations, and linear force-deformation behaviors defined by *UniaxialMaterial* elastic models in the remaining four directions. To capture the uplift behavior of the bearing, the user-specified *UniaxialMaterial* in the axial direction is modified for no-tension behavior. Coupling between vertical and horizontal directions and between vertical direction and rotation is indirectly taken into account by using expressions for mechanical properties that are derived using explicit

© The 17th World Conference on Earthquake Engineering

consideration for geometric nonlinearity due to large displacement effects [26]. By default, P-Delta moments are entirely transferred to the concave sliding surface, so that rotations of the concave surface affect the shear behavior of the bearing.

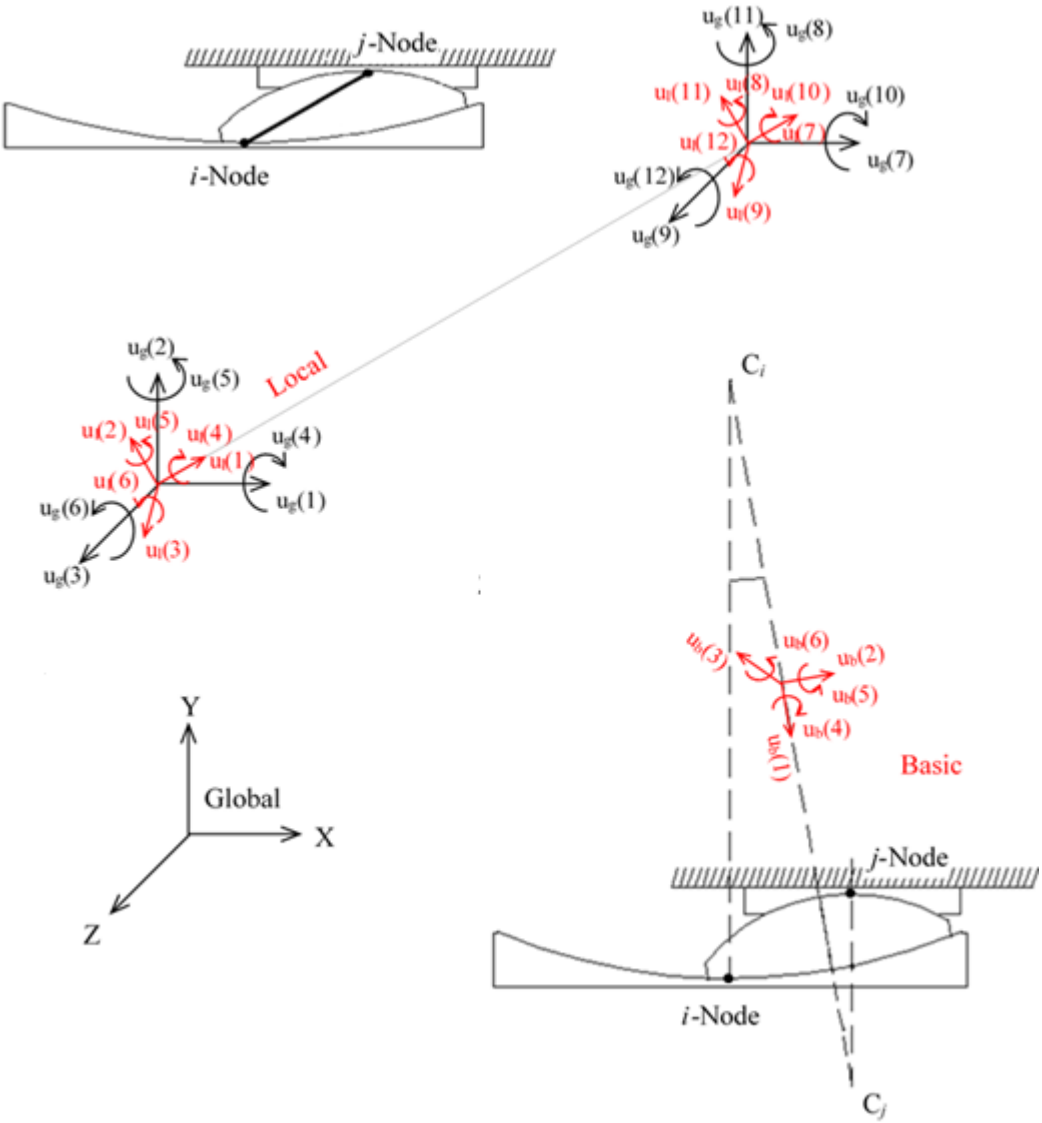

Fig. 3 – Coordinate systems of the FPS element in OpenSees; from [6]

2.2 Numerical model

The element force, displacement, and stiffness matrices are formulated at the component level in the element's basic coordinate system and transformation matrices are used to switch from basic to local and then from local to global coordinates. In the global system the contribution of each element is assembled to obtain the equations for the whole model, which are solved to obtain nodal forces and displacements. The nodal response quantities in the global system are then converted back to the element's local and basic systems to obtain forces and displacements in each element. Notations $\{u_b\}$ and $\{\mathring{u}_b\}$ are used hereinafter for the nodal displacement and nodal velocity vectors, while subscripts b and l refer to basic and local coordinates, respectively.

© The 17th World Conference on Earthquake Engineering

The software performs a numerical procedure to calculate the internal forces of the element. The description is here limited to the calculation of the shear forces, while for the other force components the standard *UniaxialMaterial* model is adopted. First, the radius in basic shear directions is calculated accounting for the deformation of the element:

$$R_y = \sqrt{R^2 - (u_b(3))^2} \qquad R_z = \sqrt{R^2 - (u_b(2))^2} \tag{2}$$

where R is the radius of curvature of the FPS, and $u_b(2)$ and $u_b(3)$ are the displacements in the basic y and z directions defined in Fig. 3(b). Noting that for small incremental displacements the two vectors $\{u_b\}$ and $\{\dot{u}_b\}$ have the same direction, tangent to the concave surface, the absolute velocity is calculated as:

$$|\dot{u}_b| = \sqrt{\left(\dot{u}_b(2)\cdot\frac{u_b(2)}{R_y} + \dot{u}_b(3)\cdot\frac{u_b(3)}{R_z}\right)^2 + (\dot{u}_b(2))^2 + (\dot{u}_b(3))^2} \tag{3}$$

The hysteretic force – displacement relationship of the FPS in horizontal direction is mathematically modeled using the theory of plasticity [26-29]. When the shear force is smaller than the friction force at the sliding surface, sliding is not engaged and the deformation is elastic. When the shear force exceeds the friction force, then sliding takes place. An iterative procedure is performed to calculate shear forces and stiffnesses in basic y and z directions. At each step, the normal force is first calculated

$$N = -q_b(1) + q_{b,Old}(2)\cdot\frac{u_b(2)}{R_y} + q_{b,Old}(3)\cdot\frac{u_b(3)}{R_z} - q_{b,Old}(2)\cdot u_l(6) + q_{b,Old}(3)\cdot u_l(5) \tag{4}$$

where $q_b(1)$ is the axial force associated to displacement $u_b(1)$ in axial direction through the *UniaxialMaterial* model, and $q_{b,Old}(2)$ and $q_{b,Old}(3)$ are the values of shear force calculated at the previous iteration. In the plasticity model, the total resisting force along each shear direction can be represented as the sum of an elastic and a hysteretic component. The stiffness associated with the elastic component is given by the ratio between the normal force and the radius

$$K2_y = \frac{N}{R_y} \qquad K2_z = \frac{N}{R_z} \tag{5}$$

and the initial stiffness of the hysteretic component is given as the difference between the (isotropic) initial stiffness of the isolator, $K1$, and the elastic stiffness

$$K0_y = K1 - K2_y \qquad K0_z = K1 - K2_z \tag{6}$$

The displacements of the hysteretic component are used as a state variable for the plasticity model, and the trial values of the hysteretic shear forces $q_{Trial}(2)$ and $q_{Trial}(3)$ are calculated as:

$$qTrial(2) = K0_y\cdot(u_b(2) - u_{b,PlasticOld}(2)) \qquad qTrial(3) = K0_z\cdot(u_b(3) - u_{b,PlasticOld}(3)) \tag{7}$$

where $u_{b,PlasticOld}(2)$ and $u_{b,PlasticOld}(3)$ are the plastic displacements at the previous iteration. Since the FPS with spherical surface has isotropic behavior in the horizontal plane, a circular yield condition is assumed. A dummy parameter Y is introduced to regulate the switching from elastic to plastic behavior:

$$Y = |qTrial| - q_{yield} \tag{8}$$

where q_{yield} is the yield force calculated in accordance with the assumed friction model and

$$|qTrial| = \sqrt{(qTrial(2))^2 + (qTrial(3))^2} \tag{9}$$

© The 17th World Conference on Earthquake Engineering

is the resultant hysteretic shear force. When $Y \leq 0$ (elastic step), the shear forces and the tangent stiffnesses for coupled shear directions are calculated as follows

$$q_b(2) = qTrial(2) + K2_y \cdot u_b(2) - N \cdot u_l(6) \qquad q_b(3) = qTrial(3) + K2_z \cdot u_b(3) + N \cdot u_l(5) \tag{10}$$

$$K_b(2,2) = K_b(3,3) = K1 \qquad K_b(2,3) = K_b(3,2) = 0 \tag{11}$$

When $Y > 0$ (plastic step), the software performs a return mapping algorithm [27] to calculate the resisting force. By assuming an associative plastic flow rule, the trial slip in either shear direction is obtained by dividing the dummy parameter Y by the initial elastic stiffness of the hysteretic component

$$dGamma_y = Y / K0_y \qquad dGamma_z = Y / K0_z \tag{12}$$

and the plastic displacement is updated

$$\begin{aligned} u_{b,Plastic}(2) &= u_{b,PlasticOld}(2) + dGamma_y \cdot \frac{qTrial(2)}{|qTrial|} \\ u_{b,Plastic}(3) &= u_{b,PlasticOld}(3) + dGamma_z \cdot \frac{qTrial(3)}{|qTrial|} \end{aligned} \tag{13}$$

Eventually the shear forces and the components of the tangent stiffness are calculated:

$$\begin{aligned} q_b(2) &= q_{yield} \cdot \frac{qTrial(2)}{|qTrial|} + K2_y \cdot u_b(2) - N \cdot u_l(6) \\ q_b(3) &= q_{yield} \cdot \frac{qTrial(3)}{|qTrial|} + K2_z \cdot u_b(3) + N \cdot u_l(5) \end{aligned} \tag{14}$$

$$\begin{aligned} K_b(2,2) &= K0_y \cdot q_{yield} \frac{qTrial(3) \cdot qTrial(3)}{|qTrial|^3} - K2_y \qquad K_b(2,3) = -K0_z \cdot q_{yield} \frac{qTrial(2) \cdot qTrial(3)}{|qTrial|^3} \\ K_b(3,2) &= -K0_y \cdot q_{yield} \frac{qTrial(2) \cdot qTrial(3)}{|qTrial|^3} \qquad K_b(3,3) = K0_z \cdot q_{yield} \frac{qTrial(2) \cdot qTrial(2)}{|qTrial|^3} - K2_z \end{aligned} \tag{15}$$

The procedure is iteratively run until the difference between the resultant shear force in two consecutive runs is less than a set tolerance level. When convergence is achieved, the shear force components are used to formulate the element stiffness matrix in basic representation [K_b] according to Equation (15). The element stiffness matrix is then transformed into the local coordinate system and "P-Delta" and "V-Delta" moment stiffness terms are added to the local force vector. The local stiffness matrix is eventually transformed into the global coordinate system and assembled to the contributions of the other elements to obtain the system of equations governing the response of the overall model.

2.3 Friction model

The standard *SingleFPSimple3d* element calculates the yield force based on the friction law coded in the associated *FrictionModel*. Different models are available in OpenSees, where the coefficient of friction is either constant (Coulomb friction) or a function of the velocity, of the axial pressure, or of both of them. The new element, called *CSSBearing_BVNC* [6], was implemented by modifying the source code of the standard element to introduce the degradation of the coefficient of friction due to heating, and the static coefficient of friction at the breakaway. The constitutive modeling is similar to the *SingleFPSimple3d* element, otherwise.

© The 17th World Conference on Earthquake Engineering

In the new formulation two plastic materials are used to account for either static or dynamic friction coefficient:

$$\begin{aligned} q_{yield} &= \mu_B \cdot N \qquad \text{for} \quad h < 1 \\ q_{yield} &= \mu_{VNC} \cdot N \qquad \text{for} \quad h \geq 1 \end{aligned} \tag{16}$$

where the variable h is increased by 1 each time the yield condition $Y > 0$ is achieved. As the analysis starts, the variable is initialized ($h = 0$), and the yield force q_{yield} is defined by the circular criterion $q_{yield} = \mu_B \cdot N$, where μ_B is the static coefficient of friction at breakaway. At the first yielding, the variable h is updated to $h = 1$, and from now on the plasticity algorithm switches to the user-defined *VNC_Friction* material model which represents the dynamic coefficient of friction. The second model calculates the yield force as $q_{yield} = \mu_{VNC} \cdot N$, where μ_{VNC} is a function of axial load, velocity and cumulated heat according to the expression

$$\mu(N,V,c) = f_{NV}(N,V) \cdot f_c(c) \tag{17}$$

Here $f_{NV}(N,V)$ is a function that accounts for the instantaneous values of axial load N and velocity V,: while $f_c(c)$ is a second function that accounts for the heat released at the sliding surface through a degradation variable c. $f_{NV}(N,V)$ is expressed accordingly to the standard exponential formulation

$$f_{NV}(N,V) = \mu_{HV}(N) - [\mu_{HV}(N) - \mu_{LV}(N)] \cdot \exp(-\alpha|\dot{u}_b|) \tag{18}$$

where μ_{LV} and μ_{HV} are the values of the dynamic coefficient of friction at low velocity and high velocity, respectively, and α determines the rate of change of the dynamic coefficient of friction with the sliding velocity [16]. The coefficients μ_{LV}, μ_{HV} and α depend on the instantaneous value of the axial load and are calculated at each iteration step according to the power law expression [30]:

$$\mu_{HV}(N) = A_{HV} \cdot N^{(n_{HV}-1)} \qquad \mu_{LV}(N) = A_{LV} \cdot N^{(n_{LV}-1)} \qquad \alpha(N) = \alpha_0 + \alpha_1 \cdot N + \alpha_2 \cdot N^2 \tag{19}$$

The variation of the coefficient of friction with heating is eventually taken into account through the degradation function f_c

$$f_c(c) = exp\left[-(c / c_{ref})^{\gamma}\right] \tag{20}$$

where c_{ref} is a parameter that regulates the rate of degradation (the smaller c_{ref}, the higher the degradation), γ is a parameter that controls the shape of the function, and c is a variable that depends on the amount of energy dissipated at the sliding surface and the distance travelled by the slider [6]:

$$c = \int_0^t N \cdot |\dot{u}_b|^2 \; dt \tag{21}$$

At each time step, the increment Δc of the variable over the time interval Δt is calculated by integration of Equation (21), and the variable is updated as $c(t + \Delta t) = c(t) + \Delta c$.

Ten material parameters are used in the implementation of the *CSSBearing_BVNC* element, namely μ_B (static coefficient of friction at breakawat), A_{LV}, A_{HV}, n_{LV}, n_{HV} (normal load-effect parameters), α_0, α_1, and α_2 (velocity-effect parameters), and c_{ref} and γ (degradation-effect parameters). Since in OpenSees software variables are dimensionless [25], the units of the materials parameters must be specified consistently with the units adopted for the fundamental physical quantities, in accordance with Table 1. Different friction models, including those already coded in OpenSees, such as *Coulomb*, *VelDependent*, and *VelNormalFrcDep* materials [25], can be derived from the novel formulation by setting the relevant parameters. More details can be found in the referenced literature [6]

© The 17th World Conference on Earthquake Engineering

Table 1 – Units of the friction model parameters of the *CSSBearing_BVNC* element

μ_B	A_{LV}	n_{LV}	A_{HV}	n_{HV}	α_0	α_1	α_2	c_{ref}	γ
–	$\left(10^{-3}\ \mathrm{N}\right)^{(1-n_{LV})}$	–	$\left(10^{-3}\ \mathrm{N}\right)^{(1-n_{HV})}$	–	s mm^{-1}	s mm^{-1} N^{-1}	s mm^{-1} N^{-2}	(10^{-3} N) mm^2/s	–

3. Response history analyses

3.1 Case study

A regular reinforced concrete, moment-resisting-frame building is considered. The structure has a double symmetric square plant of 18 by 18 m with three bays of 6 m length in both horizontal directions, and four stores at 3 m each, for a total height of 12 m, and rests on a rigid base slab (Fig. 4). The columns have square cross-section, with dimensions of 500×500 mm at the ground and the first floor, and 400×400 mm at the second and at the third floor. Rectangular (600×300 mm) beams are used at every floor. Seismic masses were evaluated by taking into account the full permanent loads plus 30% of the live loads for residential buildings according to the Italian buiiding code [31]. The total seismic weight of each floor and of the base slab is 2400 kN, resulting in a cumulative weight of the whole building of 12000 kN.

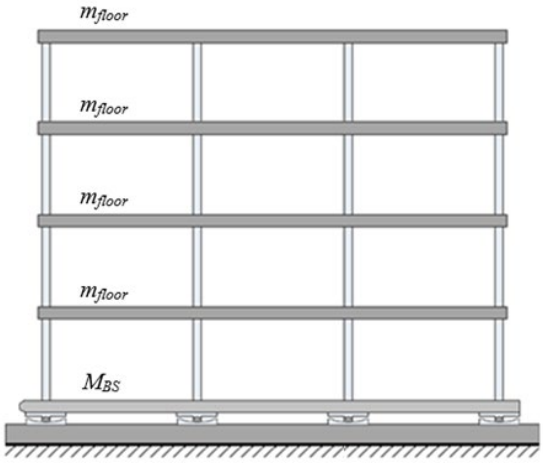

Fig. 4 – Section of the case-study building, isolated with FPSs; m_{floor} is the mass of each floor and M_{BS} is the mass of the base slab

The building is modelled in OpenSees v.2.5.4 software [25] as a moment-resisting frame with rigid joints in both directionsg. *ElasticBeamColumn* elements are used for the structural members, and the superstructure is considered to behave as a linear elastic system. The assigned modulus of elasticity of concrete is E_c = 31476 MPa (C25/30 concrete class), and the moments of inertia of the homogenized cross-sections are I_{c1} = 530512×10^4 mm^4, I_{c2} = 165627×10^4 mm^4 and I_b = 129872×10^4 mm^4 for the 500×500 mm columns, the 400×400 mm columns and the 600×300 mm beams, respectively. A *RigidFloorDiaphragm* multi-points constraint is introduced at each story to account for the in-plane stiffness of the floor slabs. The fundamental period of the superstructure is T_{SS} = 0.31 s. The internal structural damping is modeled as a stiffness proportional damping [32], with parameters assigned to achieve 5% damping ratio at a 3.5 s period.

The building is isolated at the foundation level by means of sixteen FPSs, one below each column (Fig.4). The FPSs have an effective radius R = 2500 mm, corresponding to the undamped period $Tiso$ = 3.17 s, and an initial stiffness $K1$ = 479.52 kN/mm. A floor diaphragm composed by stiff beams is created above

© The 17th World Conference on Earthquake Engineering

the isolation units in order to prevent differential displacements. The nodes at foundation level are constrained by means of rigid joints and subjected to the application of an *UniformExcitation* seismic input.

The *CSSBearing_BNVC* element is used to model the FPS isolators; the parameters assigned for the implementation of the friction model are given in Table 2 [6]. Two friction models enveloped by the *CSSBearing_BNVC* element are assumed: the BV model, accounting for breakaway and velocity effects only, and the BVC model accounting for breakaway, velocity and heating effects. For simplicity, in the case study the load effect is disregarded ($n_{LV} = n_{HV} = 1$).

Table 2 – Friction model parameters assigned in the case study; units in accordance with Table 2

model	μ_B	A_{LV}	n_{LV}	A_{HV}	n_{HV}	α_0	α_1	α_2	c_{ref}	Γ
BV	0.12	0.03	1	0.075	1	0.055	0	0	10^{100}	1.0
BVC	0.12	0.03	1	0.075	1	0.055	0	0	3.49×10^{14}	0.4

Nonlinear history response analyses are performed assuming an ordinary structure (functional class II) with nominal life of 50 years, corresponding to a reference period of 50 years, located in Naples, South Italy (14.28° longitude, 40.86° latitude), topographic category T1, soil type A (rock or other rock-like geological formation). Target elastic spectra are determined in accordance with the provisions of the Italian Building Code [31] for Damage Limitation (SLD) and Human Life Saveguard (SLV) hazard levels. For either level, a set of 21 independent bidirectional ground motions consistent with the target spectrum is selected with REXEL v3.4 beta [32] software from the European Strong-motion Database [33], and scaled to the design Peak Ground Acceleration of 0.059 g (SLD) or 0.168 g (SLV), respectively. At both levels, the average spectrum of the accelerogram set matches the Italian Building Code spectrum with a tolerance of -10/+30% in the period range 0.15 – 4.0 sec.

Baseline references for comparison are derived from nonlinear analyses performed using the standard *SingleFPSimple3d* element with *VelDependent* friction model [25] and assigned parameters: $\mu_{LV} = 0.03$, $\mu_{HV} = 0.075$, and $\alpha = 0.055$ s/mm.

3.2 Results

As Fig. 5 shows, the static coefficient of friction at breakaway can prevent small-to-medium intensity earthquakes, typical of serviceability hazard levels, from engaging the FPS isolators (Fig. 5). Indeed, sliding of the FPS is triggered when the shear force resulting from the effect of floor accelerations on the superstructure masses exceeds the frictional force at the sliding surface. When the contribution of the breakaway friction is considered, 18 out of the 21 selected ground motions at SLD are actually unable to induce sliding (14% trigger rate). However, for high intensity earthquakes, typical of ultimate limite states (SLV level), FPSs are always engaged (100% trigger rate).

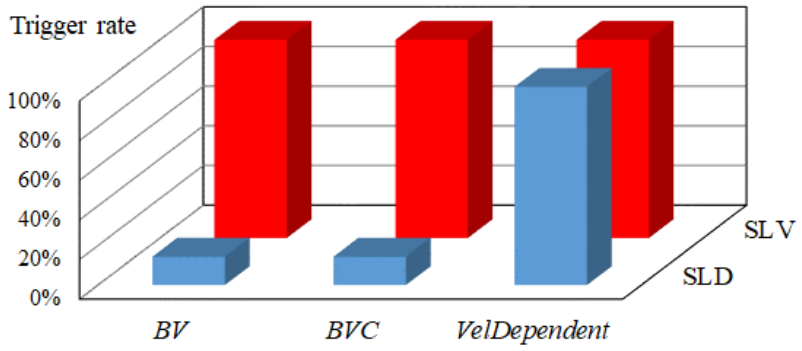

Fig. 5 – Trigger Rate of the FPS isolation system depending on earthquake intensity

© The 17th World Conference on Earthquake Engineering

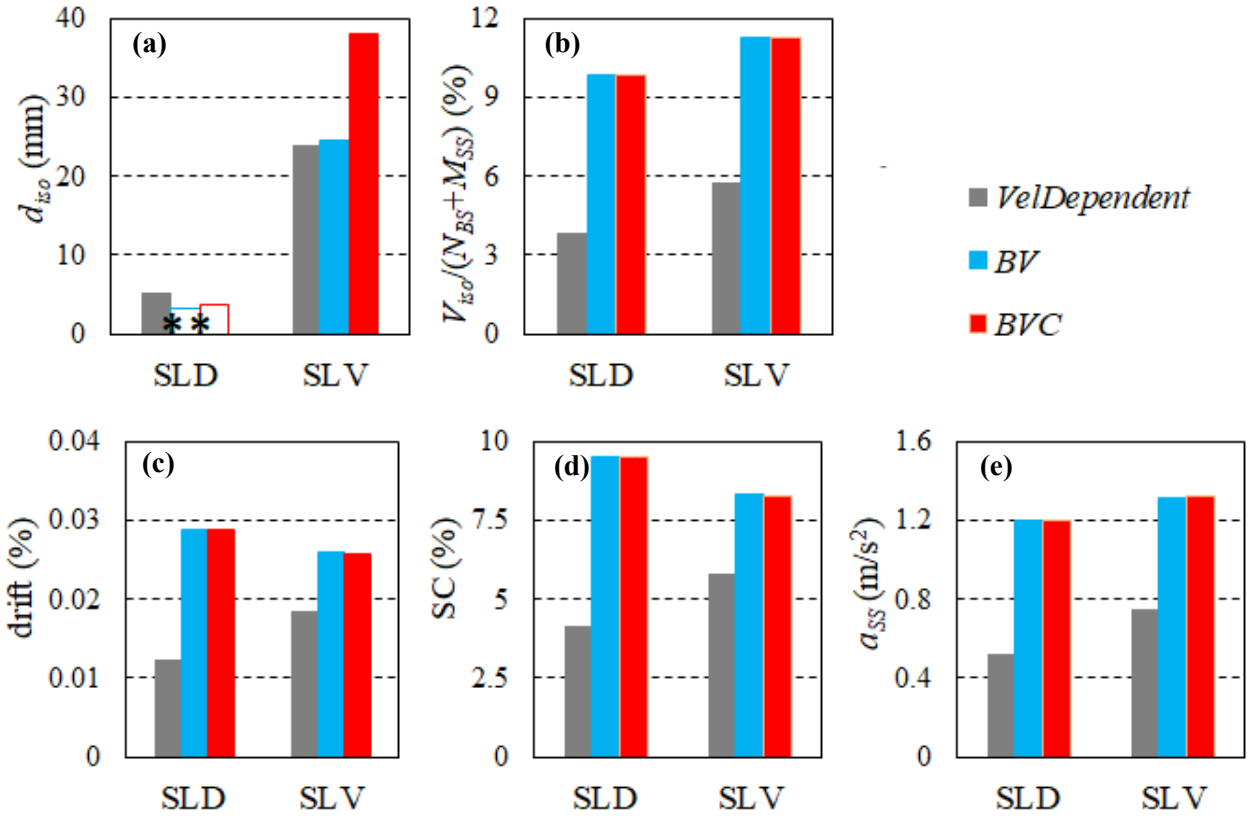

Fig. 6 – Response of the base-isolated structure at SLD and SLV hazard levels: (a) horizontal displacement of the base slab d_{iso}; (b) ratio between the overall shear force V_{iso} of the isolation layer and the total vertical load ($N_{SS} + N_{BS}$); (c) inter-story drift; (d) Seismic Coefficient (SC), i.e., ratio between the column shear and the supported seismic weight; (e) maximum floor acceleration in the superstructure a_{SS}.

Fig. 6 compares the structural response depending on the assumed friction model. The static coefficient of friction at breakaway has no practical effect on the maximum displacement at SLV level (Fig. 6(a)), as it is observed by comparing the results provided by the *BV* and the *VelDependent* models. The heating effect, which is accounted for in the *BVC* friction model, reduces the damping and hence entails an increase in the peak displacement: indeed, at SLV level, a +58% increase with respect to the baseline value is predicted, while at SLD level an evaluation of the displacement demand is not feasible because of the large number of ground motions which failed to trigger the isolators with *BV* and *BVC* friction models.

The breakaway friction induces a +155% variation in the FPS shear force at SLD level and a +95% variation at SLV (Fig. 6(b)). On the contrary, the degradation of the coefficient of friction due to heating has no effect on the maximum shear force, as the shear force at breakaway is always larger than the force developed at the maximum displacement. The average shear force predicted at SLD by the *CSSBearing_BNVC* element with breakaway friction is 71% higher than the force calculated by the standard *SingleFPSimple3d* element at SLV, and only 13% smaller that the shear force at SLV according to the new element. Therefore, dynamic analyses using the conventional FPS element and standard friction models are likely to considerably underestimate the maximum force in the isolation system.

In all the situations where the sliding isolators are not engaged, the superstructure behaves as a fixed base structure, subjected to higher accelerations than those expected according to the isolation design: a +134% increase in inter-story drift, a +130% increase in shear force in the most stressed columns, and a +128% increase in peak floor acceleration are indeed predicted at SLD from the *BV* and *BVC* models over the baseline values, Fig. 6(c-e). As already observed for the FPS shear force, internal forces and deformations of the superstructure at SLD are larger than the values predicted by the standard friction model

© The 17th World Conference on Earthquake Engineering

at SLV, namely +57% for drift, + 64% for column shear and +59% for floor acceleration. At SLV level, the static friction at breakaway produces again a large increase in superstructure drift (+41%), column shear (+43%), and maximum floor acceleration (+75%) when compared to the response predicted through the *VelDependent* friction model. The influence of heating is insignificant, demonstrating that the superstructure experiences the maximum acceleration when the isolators are in sticking condition before breakaway.

4. Conclusions

The novel *CSSBearing_BVNC* element has been formulated in OpenSees software by modifying the standard *SingleFPSimple3d* element. The new features introduced are the static friction at the breakaway and the degradation of friction due to the heat generated during the sliding motion, while the variation of the friction coefficient with the instantaneous values of axial load and velocity follows accepted practice.

A comparative evaluation performed through a case study highlights the potential of the newly developed isolator element to yield a more accurate estimation. Nonlinear response history analyses of a base-isolated building help to quantify the improved prediction capability over the standard element, with a +40% increase in estimate of superstructure drift and column shear force and a +58% increase in estimate of displacement demand at Human Life Safeguard hazard level, and possible non-activation of the sliding isolators in case of small-to-medium magnitude earthquakes.

5. References

[1] Zayas VA, Low SS, Mahin SA (1987): The FPS earthquake protection system. *Report No. 87-01*, Earthquake Engineering Research Center, Berkeley, USA.

[2] Zayas VA, Low SS, Mahin SA (1990): A simple pendulum technique for achieving seismic isolation. *Earthquake Spectra*, **6**(2), 317-333.

[3] Mokha AS, Constantinou MC, Reinhorn AM (1991): Experimental study of friction-pendulum isolation system. *ASCE Journal of Structural Engineering*, **117**(4), 1201-1217.

[4] Fenz DM, Constantinou MC (2006): Behaviour of the double concave Friction Pendulum bearing. *Earthquake Engineering and Structural Dynamics*, **35**(11), 1403–1424.

[5] Sarlis AA, Constantinou MC, Reinhorn AM (2013): Shake table testing of Triple Friction Pendulum Isolators under extreme conditions. *Report No. NCEER-13-0011*, National Center for Earthquake Engineering Research, Buffalo, USA.

[6] Gandelli E, Penati M, Quaglini V, Lomiento G, Miglio E, Benzoni GM (2019): A novel OpenSees element for single curved surface sliding isolators. *Soil Dynamics and Earthquake Engineering*, **119**, 433-453.

[7] Imbsen RA (2001): Use of Isolation for Seismic Retrofitting Bridges. *ASCE Journal of Bridge Engineering*, **6**(6), 425-438.

[8] Cardone D, Gesualdi G, Brancato P (2015): Restoring capability of friction pendulum seismic isolation systems. *Bulletin of Earthquake Engineering*, **13**(8), 2449-2480.

[9] Barone S, Calvi GM, Pavese A (2019): Experimental dynamic response of spherical friction-based isolation devices. *Journal of Earthquake Engineering*, **23**(9), 1465-1484.

[10] Constantinou MC, Tsopelas P, Kasalanti A, Wolff ED (1999): Property modification factors for seismic isolation bearings. *Report No. MCEER-99-0012*, Multidisciplinary Center for Earthquake Engineering Research, Buffalo, USA.

[11] Campbell TI, Fatemi MJ, Manning DG (1993): Friction in bridge bearings with contaminated TFE slide surface. *ASCE Journal of Structural Engineering*, **119**(11), 3169-3177.

[12] Dolce M, Cardone D, Croatto F (2005): Frictional behavior of steel-PTFE interfaces for seismic isolation. *Bulletin of Earthquake Engineering*, **3**(1), 75-99.

© The 17th World Conference on Earthquake Engineering

[13] Quaglini V, Dubini P, Ferroni D, Poggi C (2009): Influence of counterface roughness on friction properties of engineering plastics for bearing applications. *Materials and Design*, **30**(5), 1650–1658.

[14] Quaglini V, Dubini P, Poggi C (2012): Experimental assessment of sliding materials for seismic isolation systems. *Bulletin of Earthquake Engineering*, **10**(2), 717–740.

[15] Quaglini V, Bocciarelli M, Gandelli E, Dubini P (2014): Numerical assessment of frictional heating in sliding bearings for seismic isolation. *Journal of Earthquake Engineering*, **18**(8), 1198–1216.

[16] Constantinou MC, Mokha A, Reinhorn A (1990): Teflon bearings in base isolation II: modeling. *ASCE Journal of Structural Engineering*, **116**(2), 455-474.

[17] Constantinou MC, Whittaker AS, Kalpakidis Y, Fenz DM, Warn GP (2007): Performance of seismic isolation hardware under service and seismic loading. *Report MCEER-07-0012,* Multidisciplinary Center for Earthquake Engineering Research, Buffalo, USA.

[18] Lomiento G, Bonessio N, Benzoni GM (2013): Concave sliding isolator's performance under multi-directional excitation. *International Journal of Earthquake Engineering*, **30**(3), 17-32.

[19] Lomiento G, Bonessio N, Benzoni GM (2013): Friction Model for sliding bearings under seismic excitation. *Journal of Earthquake Engineering*, **17**(8), 1162-1191.

[20] Computers and Structures Incorporated (2016): *CSI Analysis Reference Manual for SAP2000®, ETABS®, SAFE® and CSiBridge*. Computers and Structures Incorporated.

[21] McKenna F, Fenves G, Scott M (2006): *Computer program OpenSees: open system for earthquake engineering simulation*. Pacific Earthquake Engineering Research Center.

[22] Tsopelas PC, Constantinou MC, Reinhorn AM (1994): 3D-BASIS-ME: Computer program for nonlinear dynamic analysis of seismically isolated single and multiple structures and liquid storage tanks. *Report NCEER-94-0010*, National Center for Earthquake Engineering Research, Buffalo, USA.

[23] Kumar M, Whittaker AS, Constantinou MC (2015): Characterizing friction in sliding isolation bearings. *Earthquake Engineering and Structural Dynamics*, **44**(9), 1409-1425.

[24] Gandelli E, Quaglini V (2018): Effect of the static coefficient of friction of curved surface sliders on the response of an isolated building. *Journal of Earthquake Engineering*, DOI: 10.1080/13632469.2018.1467353.

[25] OpenSees Manual (2017): http://opensees.berkeley.edu/wiki/index.php/Main_Page.

[26] Mosqueda G, AS Whittaker, Fenves GL, Mahin SA (2004): Experimental and analytical studies of the Friction Pendulum system for the seismic protection of bridges. *Report No. UCB/EERC-2004/01*, Pacific Earthquake Engineering Research Center, Berkeley, USA.

[27] Simo JC, Hughes TJR (1998): *Computational inelasticity*. Springer.

[28] Sivaselvan MV, Reinhorn AM (2004): Nonlinear structural analysis towards collapse simulation: a dynamical systems approach. *Report No. MCEER-2004-05*, Multidisciplinary Center for Earthquake Engineering Research, Buffalo, USA.

[29] Ray T (2013): *Modeling of multi-dimensional inelastic and nonlinear elastic structural systems*. PhD dissertation, State University of New York at Buffalo.

[30] Bowden FP, Tabor D (1964): *The friction and lubrication of solids – part II*. Oxford University Press.

[31] Ministero delle Infrastrutture (2018): *D.M. 22.03.2018, Norme Tecniche per le Costruzioni* (in Italian).

[32] Ryan KL, Polanco J (2008): Problems with Rayleigh damping in base-isolated buildings. *ASCE Journal of Structural Engineering*, **134**(11), 1780-1784.

[33] Iervolino I, Galasso C, Cosenza E (2010): REXEL: computer aided record selection for code-based seismic structural analysis. *Bulletin of Earthquake Engineering*, **8**, 339–362.

[34] Ambraseys N, Smit P, Sigbjornsson R, Suhadolc P, Margaris B (2002): *Internet-Site for European Strong-Motion Data*. European Commission, Research-Directorate General, Environment and Climate Programme, http://www.isesd.cv.ic.ac.uk/ESD.

© The 17th World Conference on Earthquake Engineering